http://tandfonline.com/inan
ISSN: 1743-5390 (print), 1743-5404 (electronic)

Nanotoxicology

Nanotoxicology, 2016; 10(8): 1041–1050
 DOI: 10.3109/17435390.2016.1144826

Taylor & Francis
Taylor & Francis Group

ORIGINAL ARTICLE

New insights into ROS dynamics: a multi-layered microfluidic chip for ecotoxicological studies on aquatic microorganisms

Volodymyr B. Koman[1], Nadia R. von Moos[2], Christian Santschi[1], Vera I. Slaveykova[2], and Olivier J. F. Martin[1]

[1]*Nanophotonics and Metrology Laboratory (NAM), Swiss Federal Institute of Technology (EPFL), Lausanne, Switzerland,* [2]*Department of Environmental Biogeochemistry and Ecotoxicology, Faculty of Sciences, Institute F.-a. Forel, Earth and Environmental Sciences, University of Geneva, Geneva, Switzerland*

Abstract

Reactive oxygen species (ROS) play an important role in the life of every cell, including cellular defense and signaling mechanisms. Continuous and quantitative ROS sensing can provide valuable information about the cell state, but it remains a challenge to measure. Here, we introduce a multi-layered microfluidic chip with an integrated optical sensor for the continuous sensitive detection of extracellular hydrogen peroxide (H_2O_2), one of the most stable ROS. This platform includes hydraulically controlled microvalves and microsieves, which enable the precise control of toxicants and complex exposure sequences. In particular, we use this platform to study the dynamics of toxicity-induced ROS generation in the green microalga *Chlamydomonas reinhardtii* during short-term exposures, recovery periods, and subsequent re-exposures. Two cadmium-based toxicants with distinct internalization mechanisms are used as stress inducers: CdSe/ZnS quantum dots (Qdots) and ionic cadmium (Cd^{2+}). Our results show the quantitative dynamics of ROS generation by the model microalga, the recovery of cell homeostasis after stress events and the cumulative nature of two consecutive exposures. The dissolution of quantum dots and its possible influence on toxicity and H_2O_2 depletion is discussed. The obtained insights are relevant from ecotoxicological and physiological perspectives.

Keywords

Cadmium, complex exposure sequences, microalgae, post-oxidative stress, quantum dots

History

Received 14 April 2015
Revised 10 January 2016
Accepted 17 January 2016
Published online 16 March 2016

Introduction

Reactive oxygen species (ROS) in biological systems are chemically reactive molecules containing activated oxygen. ROS control various physiological processes, including stress responses, signaling, and pathogen defense (Apel & Hirt, 2004; Gill & Tuteja, 2010; Henderson et al., 2009b; Yu, 1994). Therefore, a better understanding of ROS biology, their functions and dynamics, advances physiological and medical research (Gorrini et al., 2013; Nathan & Cunningham-Bussel, 2013).

In the state of cellular homeostasis ROS are in equilibrium with antioxidants (AOX). Toxicants (e.g. trace metal ions and inorganic nanoparticles) and abiotic factors (e.g. variations in temperature, salinity, UV irradiation) may directly damage cells or induce ROS generation and thereby disrupt cellular homeostasis (Finkel & Holbrook, 2000; Gill & Tuteja, 2010; Gogos et al., 2012; Nathan & Cunningham-Bussel, 2013; Rodriguez-Lorenzo et al., 2015). Oxidative stress may occur in consequence of such an imbalance of the natural ROS equilibrium. At low levels of oxidative stress, cells activate AOX and detoxification enzymes to withstand oxidative damage (Nel et al., 2013). At higher levels, inflammation and cytotoxicity overtake, often leading to cell proliferation (Nel et al., 2006). Prolonged or chronic oxidative stress can lead to organelle, membrane, lipid, protein, DNA damages and to cell death (Apel & Hirt, 2004; Cooke et al., 2003; Messner et al., 2012; von Moos & Slaveykova, 2014). Thus, the level of ROS provides information about the cell state, while the ROS production rate can predict the fate of the cell (Nathan & Cunningham-Bussel, 2013).

Here, we focus on the dynamics of ROS generation in an aquatic model microorganism, which – besides its fundamental biological interest – is also highly relevant from an ecotoxicological perspective (Balog et al., 2015; Eggen et al., 2004; Handy et al., 2008; Navarro et al., 2008; Nowack & Bucheli, 2007; von Moos et al., 2014; von Moos & Slaveykova, 2014). The latter is also of particular interest for novel nanomaterials: standard toxicity methods struggle to identify the relationship between the dose of nanomaterials and the response they induce on living entities (Nel et al., 2013). Furthermore, the toxicity mechanisms of nanomaterials are poorly understood (Clichici & Filip, 2015). However, the observation that nanomaterial surface area correlates with ROS-generating capability and toxicity has given rise to the oxidative stress paradigm (Donaldson et al., 2003; Sharifi et al., 2012). As a result, sensitive ROS-detecting techniques may shine new light on toxicity mechanisms of nanomaterials and on the progression of related diseases.

To date, common ROS-detecting techniques identify oxidative stress events, but are endpoint and qualitative (Kim et al., 2013). The rate and amount of ROS generation with respect to particular toxicants or abiotic factors remain unknown (Nel et al., 2013). However, algae exposed to ionic cadmium (Cd^{2+}) have been shown to undergo three distinct phases with different hydrogen

Correspondence: Christian Santschi, Nanophotonics and Metrology Laboratory (NAM), Swiss Federal Institute of Technology (EPFL), 1015, Lausanne, Switzerland. E-mail: christian.santschi@epfl.ch

peroxide (H_2O_2) production rates, demonstrating the complexity of cell response (Suarez et al., 2013). A major factor hindering further progress of ROS sensing lies in the difficulty to perform continuous measurements with precisely dosed stress agents. This is especially problematic for aquatic microorganisms that cannot be anchored on a surface (Bradac et al., 2009; Leptos et al., 2009).

Microfluidic chips provide an elegant solution to this challenge. Indeed, besides precise control of experimental conditions, additional advantages of microfluidics include rapid analysis, miniaturization and high throughput – all highly relevant for biological studies (Bhatia & Ingber, 2014; El-Ali et al., 2006; Thorsen et al., 2002). Platforms based on microfluidics have efficiently been used to manipulate living cells, as well as for cell culturing, spatially selective reagent delivery into cells, cell metabolism studies, drug screening and tissue engineering (Dar-Bin et al., 2009; Garcia-Cordero & Maerkl, 2014; Liu et al., 2012; Mahto et al., 2014; Tehranirokh et al., 2013; Wu et al., 2012; Zhang et al., 2014).

Here, we develop a multi-layered microfluidic chip, including hydraulically controlled microvalves and microsieves, to gain precise control over the exposure of cells to toxicants. The combination of this chip with an integrated optical biosensor allows us to quantify the dynamics and amounts of extracellular H_2O_2, which is one of the most stable ROS and therefore can be quantified extracellularly (Govindarajan et al., 2013; Henderson et al., 2009a; Jin et al., 2010; Kim et al., 2013; Suarez et al., 2013). The core of the biosensor consists of the protein cytochrome *c* (cyt *c*) printed on a porous membrane (Koman et al., 2015b). The biosensor continuously monitors the optical transmission through the cyt *c* spot, which reflects the average oxidation state of its heme group and changes upon the oxidation of cyt *c*. The obtained change in transmission can be related to the concentration of oxidizing agents, such as H_2O_2, present in solution. The porous membrane which serves as a matrix holding the cyt *c*, additionally, induces multiscattering of light, and thereby enhances its optical signal. In addition to the biosensor, the microfluidic chip enables complex exposure sequences, which, to the best of our knowledge, has not been previously performed in the context of ROS studies. The green microalga *Chlamydomonas reinhardtii* serves as a model microorganism. It is native to soil and fresh water environments around the globe (Grossman, 2007; Keeling, 2004). We studied the toxicological effects of two Cd-based toxicants: CdSe/ZnS core-shell quantum dots (Qdots), which are widely used as fluorescent labels (Dabbousi et al., 1997), and Cd^{2+}, which is known to induce oxidative stress in microalgae (Behra, 1993; Messner et al., 2012). Qdots and Cd^{2+} have different sizes, different mechanisms of internalization and induce different gene regulation pathways (Domingos et al., 2011; Misra et al., 2012; Priester et al., 2009; Sabella et al., 2014; Werlin et al., 2011). Thus, we expect distinct dynamics of ROS generation. We specifically chose Qdots and Cd^{2+} concentrations such to stimulate comparable amounts of ROS. Furthermore, intracellular ROS and membrane permeability levels were measured to supplement our extracellular measurements. Overall, this work provides new insights into the dynamics of ROS generation and toxicity.

Methods

Chemicals

All solutions, including cadmium ion solution $Cd(NO_3)_2$ (20893, Sigma), zinc ion solution $ZnSO_4{\cdot}7H_2O$ (Z0251, Sigma), CdSe/ZnS carboxyl-coated Qdots (Q21321MP, Life Technologies) or trypan blue 0.4% (15250-061, Life Technologies) were freshly prepared with distilled water for each experiment. Leached Qdots, used to investigate the effects of ionic dissolution, were aqueously diluted from the intermediate stock to 40 nM and stored for 2 days at 4 °C. Unless stated otherwise, all experiments were performed in distilled water at room temperature, i.e. 20 °C. Qdots from Life Technologies are commercially available particles with well-defined characteristics: pristine Qdots have an ellipsoid core/shell with diameters of 6 nm (minor axis) by 12 nm (major axis), the hydrodynamic diameter of carboxyl-coated Qdots is 18 nm, the size distribution is estimated at 3% and carboxyl coating prevents aggregation (Zhang & Monteiro-Riviere, 2009).

Cyt *c* sensing spots

In order to fabricate reliable and reproducible sensing elements, a microarray robot (QArray2, Genetix) was used to spot 4 mM aqueous cyt *c* (C2037, Sigma) from a 384-well plate into the substrate, consisting of a filtration membrane (GSWP 220 nm, Millipore), using a spotting pin (946MP8XB, Arrayit) with a delivery volume of 5 nl. The cyt *c* was partially crosslinked by exposing the freshly printed spots to glutaraldehyde (G5882, Sigma) in vapor phase at 100% relative humidity for 1 h and, finally, the sensing elements ready to use were stored in water at 4 °C.

Optical measurements

The cyt *c* spots were optically measured in transmission mode under white-light illumination using a 20× objective (UPlanFL 20x, Olympus, NA = 0.41) and a grating spectrometer (Triax 550, Horiba Scientific) equipped with a liquid nitrogen cooled CCD camera (Symphony, Horiba Scientific). The incident power of the light at $\lambda = 550$ nm was 10 μW/cm^2. To quantify the oxidative state, a normalized oxidative state coefficient φ was introduced (Koman et al., 2013, 2015b):

$$\varphi = \frac{A_{550}/A_{542} - A^{ox}_{550}/A^{*}_{542}}{A^{red}_{550}/A^{*}_{542} - A^{ox}_{550}/A^{*}_{542}}, \quad (1)$$

where A_{550} and A_{542} are the measured absorbance of cyt *c* at $\lambda = 550$ and $\lambda = 542$ nm, respectively. The values for A^{ox}_{550}, A^{red}_{550} and A^{*}_{542} are taken from the literature and represent the absorbance at $\lambda = 550$ nm in the oxidized and reduced state and at $\lambda = 542$ nm, respectively (Butt & Keilin, 1962). The absorbance A at $\lambda = 542$ nm is independent of the oxidative state of cyt *c* and used as reference for the normalization.

The absorbance A was calculated according to the Beer-Lambert's law: $A = -\log(I/I_0)$, where I and I_0 refer to the light intensity measured after the light passed through the membrane with and without cyt *c*, respectively (Koman et al., 2015a). The H_2O_2 concentration $C_{H_2O_2}$ at a given time t was quantified using the following equation (Koman et al., 2015b):

$$C_{H_2O_2} = -\frac{d\varphi/dt}{k\varphi}, \quad (2)$$

where k is the reaction rate constant for the oxidation of cyt *c* by H_2O_2 in water ($k = 0.24\,min^{-1}{\cdot}\mu M^{-1}$). For clarity, the initial values of φ at $t = 0$ were normalized with respect to the control experiment. As can be seen from Equation (2), this does not affect the calculated $C_{H_2O_2}$ values. Experiments performed on blank samples, in the absence of H_2O_2, revealed a limit of detection (LOD) of 40 nM.

Microfluidics

All microfluidic layers (Figure 1a) were prepared from poly-dimethylsiloxane (PDMS) (10:1 ratio of PDMS/curing agent, if not stated otherwise) using casting technique. The corresponding molds were fabricated by standard photolithography in SU-8

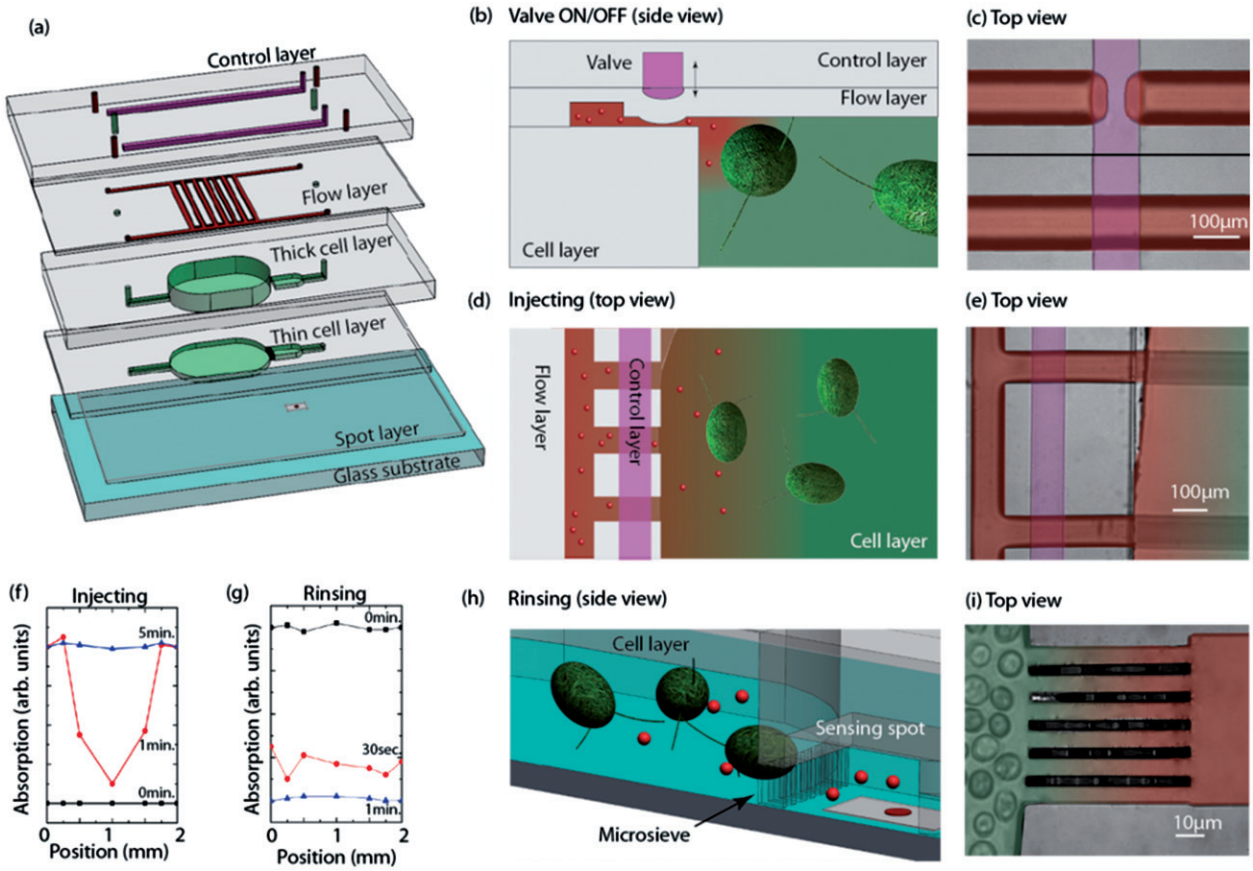

Figure 1. (a,b,d,h) Schematic drawings and (c,e,i) microscope pictures of the multi-layered microfluidic chip: (a) full chip configuration; (b,c) valve operation to control the connection between flow and cell layers; (d,e) injection mode when the toxicant enters into the cell layer; (h,i) rinsing mode when the toxicant leaves the cell layer through the microsieve. Colors in the microscope images are artificial. The red spheres represent the toxicant and the green ellipsoids the algae. Time evolution of trypan blue absorption (4 µM concentration in the flow layer) across the cell layer shown during (f) injecting and (g) rinsing.

photoresist (except the flow layer where AZ9260 photoresist was used) (Huang et al., 2009). A spot layer (100 µm thickness) was deposited by spin-coating PDMS at 500 rpm for 40 s, followed by manual hole cutting to accommodate the sensing spot. The cell layer consists of two layers of 40 µm and 1 mm thicknesses. The thick cell layer (1 mm thick with 300 µm thick channels) containing the input channel (300 µm wide) and cell compartment (2 mm wide) was prepared by pouring the appropriate amount of PDMS onto the mold. The thin cell layer (40 µm thick with 10 µm thick channels) contains the same base-pattern with additional microsieve (5 µm period, 100 µm long) and was deposited by spin-coating PDMS at 8000 rpm for 5 min (Figure 1h and i). The flow (20:1 ratio) and control layer (5:1 ratio) had a thickness of 40 µm (spin-coating at 5000 rpm for 5 min) and 1 mm (pouring), respectively. Both of these layers had 10 µm thick and 100 µm wide channels (Figure 1d and e). After pouring the PDMS onto the molds, all layers were prebaked for 30 min at 80 °C. The thick cell and control layers were tailored and separated from the molds. Subsequently, the thick cell layer was carefully aligned and placed onto the thin cell layer, while the control layer – onto the flow layer. These two assemblies were baked at 80 °C overnight. After the prebaking step the PDMS is not entirely cross-linked and, consequently, the subsequent full baking process strongly joins the layers lying on each other. After baking, an additional thin PDMS layer was added on top of the cell layer (spin-coating at 5000 rpm for 3 min). The cell compartment was manually carved through both thick and thin cell layers. The attached control and flow layers were aligned with respect to the cell layer and baked at 80 °C for 2 h with the freshly spin-coated PDMS layer serving as bonding material. Finally, the spot layer was placed on the microscope slide and baked at 80 °C overnight. Prior to the measurements, a sensing spot was inserted into the opening in the spot layer. Then, the microfluidic chip was placed on top and the center of the channel, where the measurements take place, was carefully aligned with respect to the spot. At last, the entire system was clamped between two metallic plates with appropriate openings enabling the optical measurements.

Algae culture

The green alga *C. reinhardtii* strain (CPCC 11) was provided by the Canadian Phycological Culture Center. Axenic cultures were grown in Tris-Acetate-Phosphate (TAP) liquid growth medium and maintained in an incubator (Infors, Bottmingen) at 20 °C with a 24 h illumination regime (114.2 µmol·phot/(m^2·s)) and constant rotary shaking (120 rpm). The culture was regularly re-inoculated in fresh growth medium and cells were harvested in mid-exponential phase. Prior to the experiments, algae were gathered by centrifugation (3000 rpm, 5 min), rinsed twice, transferred to distilled water and adjusted to a final concentration of approximately 2×10^6 cells/ml. The cell concentration was optically determined at 680 nm using a pre-calibrated photo-spectrometer (Ultrospec III, Pharmacia).

Injecting and rinsing

All microfluidic operations were performed using a liquid pump (Xcalibur, Tecan) controlled via the Labview software. Prior to use, the microfluidic chip was rinsed with distilled water at a

constant flow rate (2 mm/s). The integrated microfluidic valves operate according to the following principle: an increase of the channel pressure in the control layer (by applying a gentle flow of 0.1 mm/sec for 10 s) expands the channel, closing the corresponding cross-sections in the flow layer (Figure 1b–i). The valves were held in the closed state while the algae suspension was carefully injected into the cell layer (0.5 mm/s) until they reached the cell compartment. Then, the flow in the cell layer was stopped. The cell compartment layer (1 mm high, 2 mm wide and 1 cm long, total volume of 20 µl) contains approximately 40,000 cells, when fully filled.

In a preparatory step, the analyte was introduced into the flow layer with the valve in the closed state (2 mm/s). Subsequently, the valve was opened and the analyte was gently injected from the flow layer into the cell layer by applying the flow at both ends of the flow layer channels (0.1 mm/s for 3 s). After a time lapse of 50 s to allow diffusion, the valve was closed and a new injection cycle started. Since the channels in the flow layer have a much smaller volume than the cell layer, in order to efficiently inject analyte, we proceeded in the following manner: the injection cycle was repeated five times, the first three times by injecting an analyte concentration 10× higher than the final concentration, followed by two injections with the final analyte concentration.

To remove the analyte from the cell layer, the microfluidic valve was closed and a gentle flow of distilled water (0.2 mm/s, for 1 min) was applied. Subsequently, a backward flow (0.2 mm/s for 3 s) was applied to help the cells spread out again into the cell compartment. In this paper, trypan blue was used as an analyte for the diffusion experiments and ionic Cd and Qdots, for the algae experiments. Unless stated otherwise, ''exposure'' means that the analyte is injected and remains in the biosensor cell compartment during the whole experiment.

To exchange the sensing spots between two consecutive series of measurements, the algae were removed from the cell layer, the microfluidic chip was opened, the sensing spot exchanged, the microfluidic chip closed and the algae re-introduced. This procedure takes approximately 3 min.

Intracellular ROS and membrane integrity measurements

To complement the continuous measurements of H_2O_2 performed with the microfluidic chip, we also measured intracellular ROS and membrane integrity as representatives of conventional endpoint assays for oxidative stress.

Intracellular ROS evaluations are based on the intensity of the fluorescent signal stemming from intracellularly de-esterified H_2DFC-DA (dihydrodichlorofluorescein diacetate) reacting locally with generated ROS (Kim et al., 2013). Intracellular ROS measurements were carried out using cell samples (cell density of *ca.* 2×10^6 cells/ml) incubated with 20 µM CM-H_2DCFDA (35848, Sigma) for 30 min in the dark. Their fluorescent intensity was measured in a multi-well plate reader (Safire2, Tecan) at $\lambda = 525$ nm using an excitation wavelength of $\lambda = 495$ nm.

To assess membrane permeability the samples were incubated with 12 µM propidium iodide dye (P4170, Sigma) for 30 min in the dark. The fluorescent intensity at $\lambda = 617$ nm was measured using an excitation wavelength at $\lambda = 536$ nm. Positive controls for both, membrane permeability and intracellular ROS assays, were run by exposing the algae for 30 min to 10 mM H_2O_2 prior to the incubation with dyes.

Determination of dissolved and cell-associated metal contents

To determine the amount of dissolved Cd^{2+} and Zn^{2+}, 3 ml of Qdots suspension (5 nM) were put in dialysis bags (1 kDa Uptima H1-18-10, CelluSep) and immersed in 3 ml of distilled water for the time of experiment as indicated below.

ICP-MS (Thermo Finnigan) was used for the quantitative differentiation between extracellular and cell-associated (i.e. the sum of intracellular material and material sticking to the cell membrane) amounts of metallic elements. To determine the cell-associated Cd and Zn amounts, 10 ml of algae dispersion was rinsed and digested until the solution became colorless (0.2 ml of HNO_3 at 85 °C) prior to the ICP-MS analysis. Measured ICP-MS amounts were converted to concentrations.

Results

Microfluidic system

To gain precise control over the exposure of algae to toxicants, we designed and fabricated a microfluidic chip, which consists of five layers (Figure 1a). The spot layer accommodates the sensing spot and guarantees optimal integration with the rest of the chip. The sensing spot lies in the proximity of the cell layer, so that H_2O_2 reaches the spot sufficiently fast by diffusion (Supplementary Figure S1 and S2), but is well-separated from the algae to exclude optical interference. The cell layer serves as a cell compartment during measurements (thick part) and contains a microsieve (thin layer), which retains algae during rinsing (Figure 1h and i). The toxicant enters the chip through the flow layer which is connected to the cell layer (Figure 1d and e). This connection is controlled by microfluidic valves in the control layer (Figure 1b and c).

To visualize the diffusion of the injection process in the cell layer, we performed separate experiments in which we injected 4 µM of trypan blue dye into the flow layer according to the procedure described in the Methods section (while the cell layer was filled with distilled water). Absorption measurements indicate that the dye uniformly spreads across the cell layer within 5 min (Figure 1e) and after 1 min rinsing, the dye is completely removed (Figure 1f).

We further demonstrate efficient injection mechanisms by observing similar H_2O_2 responses from algae exposed to 500 nM Cd^{2+} through the injection in the microfluidic system and algae exposed to 500 nM Cd^{2+} prior to their introduction into the cell layer (Supplementary Figure S3). Furthermore, algae exposed to 100 nM Cd^{2+} showed no generation of H_2O_2 after washing away the Cd^{2+} immediately after injection, demonstrating the effectiveness of the rinsing procedure (Supplementary Figure S4).

Exposure to Cd^{2+}

We used this microfluidic chip to control algae exposure to Cd^{2+}. Fresh water typically contains levels of $Cd^{2+} < 10$ nM, but concentrations up to 100 nM may occur due to environmental disturbances, such as acid rain (Nordberg et al., 2014). Therefore, two different Cd^{2+} exposure levels were investigated to study oxidative stress: 100 nM an environmentally relevant and 500 nM, a presumably toxic concentration.

We continuously measured extracellular H_2O_2 released from exposed algae using the sensing spot that monitors the cyt *c* oxidative state (Koman et al., 2015b; Suarez et al., 2013). As described above, extracellular H_2O_2 oxidizes cyt *c*, causing its absorption to change. We optically monitored this change and quantified it using the oxidation state coefficient φ (Equation 1), further calculating the H_2O_2 concentrations present in solution (Equation 2). Control experiments with unexposed algae did not show any H_2O_2 generation (blue lines in Figure 2a and c). Differential measurements eliminate the effect of interference between Cd^{2+} and the cyt *c* sensing spot (Supplementary Figure S5).

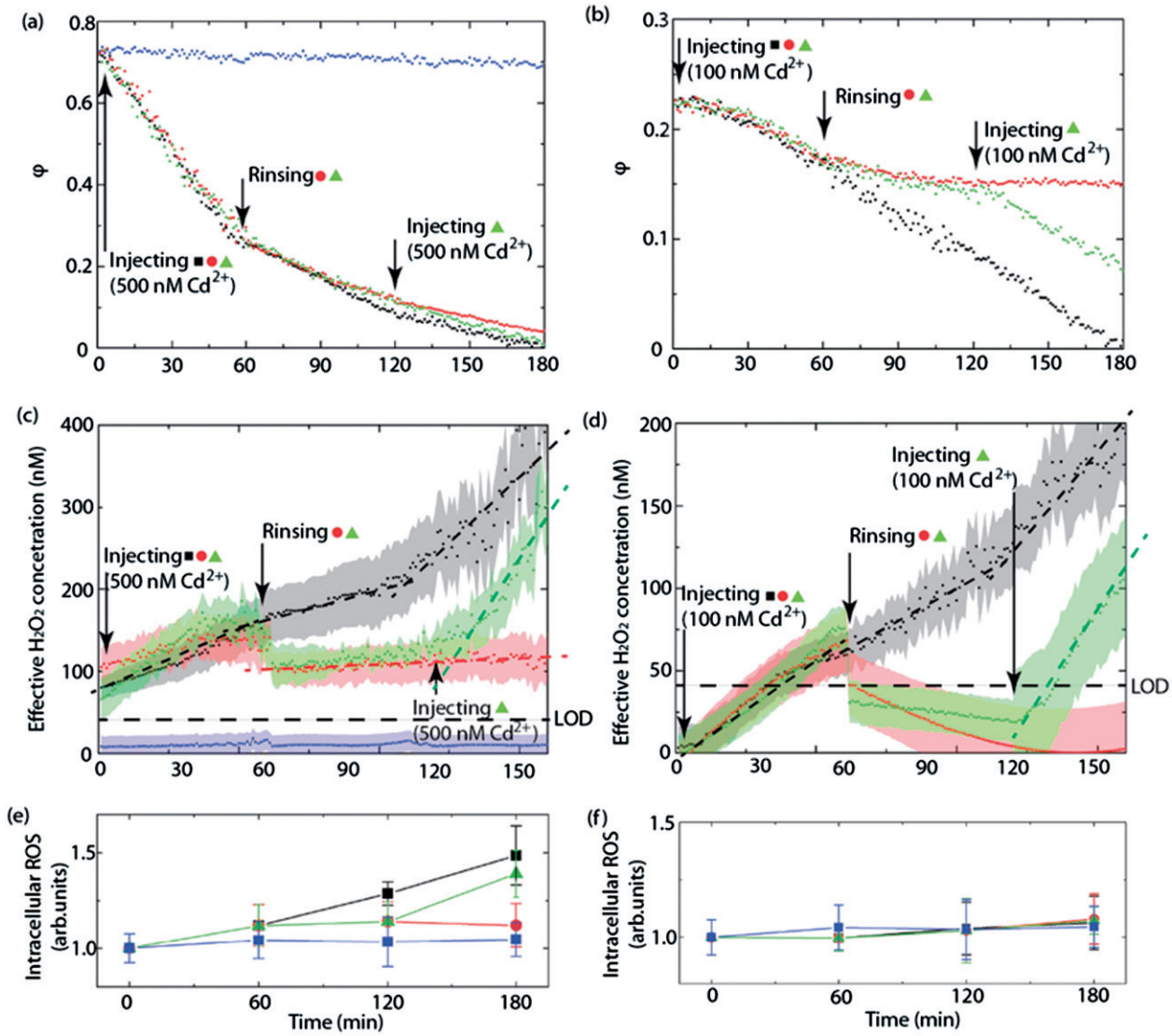

Figure 2. Algae exposure to Cd^{2+}. Oxidative state coefficient φ vs. time for: (a) 500 nM and (b) 100 nM exposure cycles. (c,d) Extracellular H_2O_2 concentration $C_{H_2O_2}$ converted using Equation (2). The shaded areas represent the standard deviation over three samples. The horizontal black dashed line represents the LOD at 40 nM. Other dashed curves are linear fits. Intracellular ROS measured by fluorescence for (e) 500 nM and (f) 100 nM Cd^{2+} exposures in identical cycles as in (a) and (b) (the same colors as in (a) are used: blue squares correspond to unexposed algae, black squares to algae exposed for 3 h, red circles to algae rinsed after 1 h exposure and the green triangles correspond to re-exposed algae, which were rinsed after the first 1 h exposure). Error bars represent the standard deviation of nine samples. Tukey multiple comparisons of means are available in Supplementary Tables S1 and S2.

When exposed to 500 nM of Cd^{2+}, algae rapidly produced H_2O_2: immediately after the injection, we detected $C_{H_2O_2} = 80$ nM, which then increased to 150 nM after 60 min (1.2 nM/min), to 220 nM after 120 min (1.2 nM/min) and to 380 nM after 160 min (4.0 nM/min, black lines in Figure 2a and c). The H_2O_2 production rates are estimated with linear fits. The injection procedure duration – in the order of 5 min – explains the non-zero $C_{H_2O_2}$ value at the beginning of the experiment. Algae exposure to the lower concentration of Cd^{2+} (100 nM) induced similar, but slower responses: $C_{H_2O_2}$ reached 70 nM after 60 min (1.1 nM/min), 130 nM after 120 min (1.0 nM/min) and 200 nM after 160 min (1.6 nM/min, black lines in Figure 2b and d).

$C_{H_2O_2}$ dropped to 100 nM when, after 60 min exposure to 500 nM of Cd^{2+}, the cell layer was rinsed to remove both the produced H_2O_2 and injected Cd^{2+}. This level remained constant during the following 100 min (red line in Figure 2c). We refer to this type of experiment as post-stress experiments. Post-stress after exposure to 100 nM of Cd^{2+} was even more pronounced: $C_{H_2O_2}$ dropped below the detection limit (red line in Figure 2d).

When, after 60 min of post-stress, algae were re-exposed to the same concentration of Cd^{2+} as during the first exposure, their responses were stronger. In particular, for 500 nM of Cd^{2+} re-exposure, $C_{H_2O_2}$ increased from 100 nM to 300 nM within 40 min (5.0 nM/min, green line in Figure 2c); for 100 nM of Cd^{2+} re-exposure, $C_{H_2O_2}$ increased from 20 nM to 110 nM within 40 min (2.3 nM/min, green line in Figure 2d). Due to the strong oxidation of the cyt *c*, the sensing spots were exchanged after every hour of measurement. During the last 20 min of the experiment, φ nearly reached zero (Figure 2a and b) and could not be used for a reliable $C_{H_2O_2}$ determination; hence data stop at $t = 160$ min in Figure 2c and d.

For 500 nM Cd^{2+}-exposures intracellular ROS levels match the trends of extracellular H_2O_2 well (Figure 2e). In contrast, for 100 nM Cd^{2+}-exposures intracellular ROS levels became statistically significant only after an exposure over 3 h and showed similar values for both, post-stress and continuous exposures

(Figure 2f). Complementary membrane permeability measurements revealed that the algae membrane was affected, but the algae remained alive after 3 h of Cd^{2+} exposure as compared to positive controls with 10 mM H_2O_2 exposure (Supplementary Figure S6).

Exposure to Qdots

Similarly to Cd^{2+}, we exposed algae to CdSe/ZnS Qdots using the microfluidic chip for continuous measurements of the production of extracellular H_2O_2. Control experiments with 5 and 20 nM of Qdots showed no interaction with the cyt *c* sensing spot (Figure 3a). Algae exposed to 5 nM, respectively 20 nM, Qdots generated H_2O_2 concentrations comparable to Cd^{2+}, reaching $C_{H_2O_2} = 75$ nM, respectively 100 nM, after 60-min exposure time (Figure 3a and b). In contrast to the Cd^{2+} exposures, we observe an H_2O_2 induction period: higher concentration of Qdots led to a shorter induction period (10 min period for 20 nM of Qdots and 30 min for 5 nM, respectively). When exposed to 5 nM of leached Qdots, algae generate H_2O_2 at a faster rate reaching $C_{H_2O_2} = 150$ nM within 1 h and shorter induction period (~20 min) as compared to an exposure to 5 nM of fresh Qdots. To explain the difference between the experiments performed with fresh and leached Qdots, we measured the total (27.5 μM of Cd and 13.8 μM of Zn, corresponding to 5 nM of Qdots) and the dissolved amounts of Cd^{2+} and Zn^{2+} in the dispersion by ICP-MS. In the absence of the algae, only minute quantities of Cd^{2+} and Zn^{2+} (10 nM and 150 nM, respectively) are present in the 3 h-old Qdot dispersion (Figure 3g). In contrast, the 2-day-old Qdots release 20 nM of Cd^{2+} and 13 μM of Zn^{2+}, indicating the total dissolution of the ZnS-shell, while the CdSe-core remains mostly intact. Additional experiments were performed, exposing algae to 13 μM of Zn^{2+} leading to a production by the algae of 60 nM H_2O_2 within 1 h; on the other hand, exposure to 1 μM Zn^{2+} did not induce any measurable response (Figure 3c and d). This is consistent with the fact that Zn^{2+} is an essential element for algae (Hanikenne et al., 2009).

A different behavior was observed for longer exposure times. For instance, exposing the algae for 120 min to 5 nM Qdots, $C_{H_2O_2}$ started to decrease after 90 min and, finally, dropped to the LOD (green curves in Figure 3e and f). In the post-stress case, the $C_{H_2O_2}$ values were below the detection limit (black curves in Figure 3e and f). ICP-MS measurements of the cell-associated elements revealed 300 nM (0.5 amole/cell) Cd^{2+} and 1.15 μM (2.0 amole/cell) Zn^{2+}, after 2 h exposure to 5 nM Qdots (Figure 3h). On the other hand, the corresponding intracellular ROS levels increased with time, including in the post-stress case (Figure 3i).

Discussion

Difference between measuring intracellular ROS and extracellular H_2O_2

Under steady state conditions, AOX scavenge ROS in biological systems (Gill & Tuteja, 2010). If cell homeostasis is disturbed, for example in this work by the presence of Cd^{2+}, unbalanced ROS spread around the cell, damaging nucleic acids, oxidizing proteins and causing lipid peroxidation (Foyer & Noctor, 2005). Due to their short lifetime (in the order of microseconds), ROS also transform into their most stable representative, which is H_2O_2 (Jin et al., 2010). Unbalanced H_2O_2 is excreted through the cell membrane. Thus, the concentration of extracellular H_2O_2 depends on the concentration of overproduced ROS. Indeed, during the exposure to Cd^{2+}, H_2O_2 was found outside algae, indicating oxidative stress (Koman et al., 2015b). As a result, continuous extracellular H_2O_2 measurements, quantifying the overproduction of ROS, complement endpoint intracellular ROS levels.

H_2O_2 excretion

We found that the exposure of algae to Cd^{2+} induces continuous H_2O_2 release during 1 h (black curves in Figure 2c and d). Cd^{2+} is rapidly taken up by the algae and stimulates ROS generation (Hanikenne et al., 2009). Consequently, the concentration of ROS exceeds that of AOX and oxidative stress sets in (Hanikenne et al., 2009; Lamelas et al., 2009). This is reflected by elevated intracellular ROS (Figure 2e) and extracellular H_2O_2 levels (Figure 2c) when the algae are exposed to 500 nM of Cd^{2+}. At a lower concentration of Cd^{2+} (100 nM) intracellular ROS levels do not rise (Figure 2f), even though algae excrete H_2O_2 (Figure 2d). This indicates that excretion of intracellular ROS in the form of H_2O_2 represents a pathway for maintaining stable intracellular ROS levels. However, the capability of such excretion has to be limited. Indeed, at elevated stress (exposure to 500 nM of Cd^{2+} in this work), the algae probably cannot efficiently excrete all excess intracellular ROS, which is reflected by elevated intracellular ROS levels.

There are several hierarchical levels of oxidative stress (Nel et al., 2006). During the first 2 h of Cd^{2+} exposure, $C_{H_2O_2}$ increases with a similar rate, but longer exposure results in an increased release rate (Figure 2c and Table 1). At this point, algae probably enter a new phase of oxidative stress with inflammation mechanisms taking over the AOX defense (Nel et al., 2006). Indeed, besides ROS production, Cd^{2+} exposure also stimulates production of various AOX, including glutathione (Aravind & Prasad, 2005; Sun et al., 2005).

In order to measure the post-stress behavior, both extracellular Cd^{2+} and H_2O_2 were removed after 1 h from the microfluidic chip as described above. Thus, when the microfluidic chip – containing algae treated with 100 nM Cd^{2+} – is rinsed, the extracellular $C_{H_2O_2}$ drops to the detection limit (red curve in Figure 2d). In the case of 500 nM Cd^{2+} exposure, we observe a drop in $C_{H_2O_2}$ to 100 nM (red curve in Figure 2c). These non-zero values of $C_{H_2O_2}$ are associated with elevated intracellular ROS levels: the algae continue to excrete H_2O_2 during the washing period (~5 min) (Figure 2c–f). This indicates that the H_2O_2 concentration gradient over the cell wall – created during the rinsing step – sustains the excretion. After a rapid jump during the rinsing step, both extracellular H_2O_2 and intracellular ROS concentrations remain stable. These results suggest that algae have the ability to reestablish rapidly the ROS/AOX balance.

A consecutive exposure to the same concentration of Cd^{2+} shows higher $C_{H_2O_2}$ generation rates (green curves in Figure 2c and d) with respect to the first exposure (Table 1). Thus, we observe that the rate and extent of ROS generation depend not only on the given toxicant exposure but also on previous events. This effect can be associated with intracellular fate of Cd^{2+} (Domingos et al., 2011). Once inside the algae, Cd^{2+} can substitute other ions like Ca^{2+}, Cu^{2+}, and Zn^{2+}, disrupting cellular functions (Suarez et al., 2013; Wang et al., 2004).

Qdots-induced oxidative stress

Both intracellular ROS and extracellular $C_{H_2O_2}$ levels increased within the first hour of algae exposure to CdSe/ZnS Qdots as displayed in Figure 3b and f. The increase of ROS can be attributed to cell-associated Cd and Zn (Figure 3h). However, ICP-MS measurements do not discriminate if the cell-associated metals were present in the form of Qdots or dissolved metal ions. We attempted imaging experiments in order to detect the fluorescent Qdots inside the algae, but obtained no conclusive results because the fluorescence of algae overlaps with that of Qdots (data not shown). As indicated by ICP-MS, pristine Qdots have a 2:1 concentration ratio of Cd and Zn (Figure 3g). Since only 300 nM of cell-associated Cd was detected, we can estimate

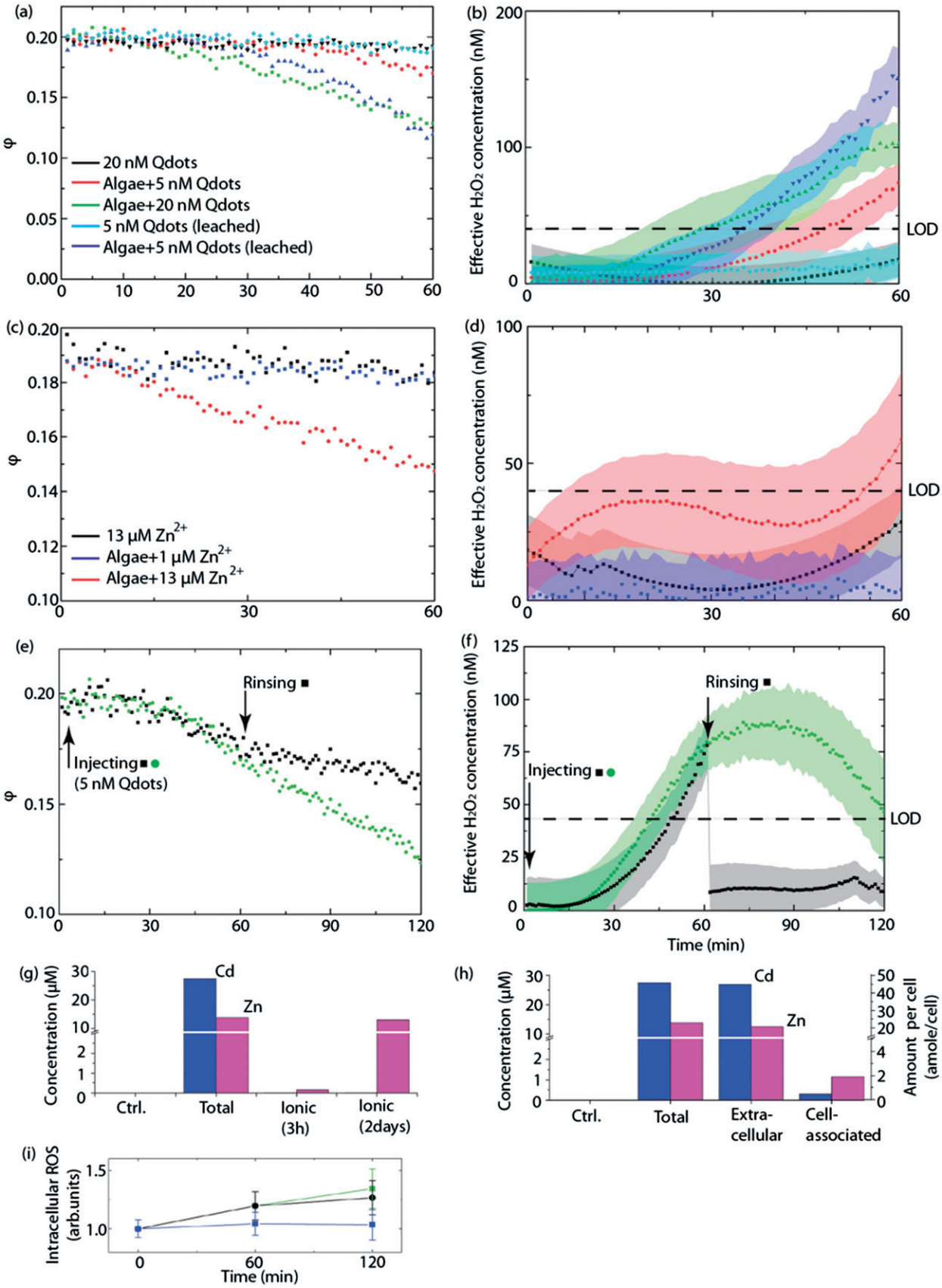

Figure 3. Algae exposure to Qdots. (a) Oxidative state coefficient φ vs. time when exposed to 5 nM, 20 nM, and 5 nM leached Qdots in the presence and absence of algae. (b) Extracellular H_2O_2 concentration $C_{H_2O_2}$ converted using Equation (2). (c,d) Exposure to Zn^{2+}. (e,f) Exposure to 5 nM Qdots. The green circles correspond to algae exposed for 2 h and the black squares show algae rinsed after 1 h exposure. The shaded areas show the standard deviation of three samples. The black dashed line shows LOD at 40 nM. (g) ICP-MS measurements for total and dissolved Cd and Zn of 5 nM of Qdots. (h) ICP-MS measurements of extracellular and cell-associated Cd and Zn after a 2-h exposure of algae to 5 nM Qdots. The right axis (amount per cell) is only for cell-associated category. (i) Intracellular ROS of 5 nM Qdots exposures for identical cycles as in (e) (the same colors as in (a) are used, blue corresponds to unexposed algae). The error bars represent the standard deviation of nine samples. Tukey multiple comparisons of means are available in Supplementary Table S3.

Table 1. Extracellular C_{H_2O2} rates (in nM/min) for Cd^{2+} exposures to algae.

Exposure	Hour	500 nM Cd^{2+}	100 nM Cd^{2+}
1st	1st	1.2	1.1
	2nd	1.2	1.0
	3rd	4.0	1.6
2nd	1st	5.0	2.3

the upper limit of 150 nM for Zn in the form of Qdots and, in turn, more than 1 µM must be in the ionic form (Figure 3h). This corresponds to a 6-fold higher amount of dissolved Zn^{2+} in the presence of algae as compared to pure water, which previously has been attributed to the change of the pH level in the vicinity of algae (Domingos et al., 2011; He et al., 2015; Sabella et al., 2014; Slaveykova & Startchev, 2009; Slaveykova et al., 2009). Control experiments with such quantities of Zn^{2+} did not induce any extracellular H_2O_2 (Figure 3d). Therefore, elevated ROS and $C_{H_2O_2}$ levels – observed in Qdots exposure – are mediated via cell-associated Qdots/Cd^{2+}.

If the Qdots exposure to algae is extended, $C_{H_2O_2}$ stops to increase during the second hour and even decreases toward the end of the experiment (green curve in Figure 3f). The latter effect might be connected with CdSe/ZnS Qdots converting H_2O_2 into water (Bae et al., 2004; Dennany et al., 2011; Hu et al., 2010; Jiang & Ju, 2007). Moreover, this conversion can be much more efficient after dissolution of the ZnS shell. Indeed, one of the functions of Zn-shell in Qdots is to remove electron-hole traps at the surface of the Cd-core (Reiss et al., 2009) and to confine the excited electrons in the core of Qdots (Dabbousi et al., 1997). However, as discussed above, cell-associated Qdots are characterized by enhanced dissolution. Keeping this in mind, we propose the following scenario: once the ZnS shell forfeits its sealing capability, Cd^{2+} leaches into the algae and triggers oxidative stress, leading to an increase of intracellular ROS levels (Figure 3i). The presence of the induction time (Figure 3f), which was not observed in the Cd^{2+} experiments, further supports this toxicity mechanism. Concurrently, after the CdSe core is stripped, an enhanced depletion of H_2O_2 sets in as discussed above. Comparing 500 nM Cd^{2+} and Qdots exposures, they both stimulate intracellular ROS production. However, in contrast to 500 nM Cd^{2+} exposure, $C_{H_2O_2}$ is well below the detection limit (black curve in Figure 3f) in the post-stress after Qdots exposure. This further strengthens the presumption that Qdots deplete H_2O_2. As a result, measured H_2O_2 concentrations in Qdots experiments are underestimated since H_2O_2 is partly destroyed.

Scope of application

The developed microfluidic chip is a multifaceted platform that allows complex sequences of analyte adding, mixing, and rinsing. This is a real breakthrough in the ecotoxicological experimentations, enabling completely new dynamic experiments. Since injection channels have dimensions of 100 µm, there is no restriction of analytes: various ions, nano- or even microparticles can be injected. In this work we established and optimized the method using Qdots and Cd^{2+} ions as model contaminants, but in future other more commonly spread toxicants including engineered nanomaterials, toxic metals, and synthetic organics should be tested. These include nanoparticles that contain silver, zinc, silica, titanium, gold, carbon nanotubes, and fullerenes (Weinberg et al., 2011). Even though injection and rinsing are not immediate, cellular ROS generation is slow enough for our sensor to capture the full dynamics. Besides direct exposure to toxicants the platform can be expanded to study effects of various illumination regimes and electromagnetic fields, thanks to the transparency and dielectric properties of PDMS. Since the system is quite complex careful control experiments are highly recommended: interference might occur between toxicants and the cyt *c* spot and toxicants and the released H_2O_2 in the given media. Differential measurements in the presence and the absence of toxicants may help eliminate such effects. Also, during prolonged experiments the cyt *c* spots might undergo full oxidation and have to be exchanged, which will disrupt ongoing measurements. Due to the relatively high thickness of the cell layer (300 µm), the microfluidic chip can accommodate cells even bigger then algae. On the other hand, we can also work with smaller cells by reducing the size of microsieve (photolithographically made microsieves can be reduced down to 0.5 µm, while other nanofabrication methods can provide even smaller features). The multi-layered microfluidic chip is fabricated using the cheap and standard PDMS line, making it highly accessible for various biological and ecotoxicological studies. The whole measurement setup, which operates both the microfluidic chip and the integrated biosensor, is compact and portable (Koman et al., 2015b).

Conclusions

We have presented a microfluidic chip with an integrated optical biosensor, which enables continuous measurements of extracellular H_2O_2 with a LOD of 40 nM. These measurements give access to the dynamics of the cell state providing precious information of cellular biochemical processes. The method is noninvasive, which is a major advantage compared to frequently used fluorescent probes (Kalyanaraman et al., 2012). The integrated microfluidic valves allow complex experimental sequences of analyte adding, mixing, and rinsing. The installed microsieves confine algae inside the microfluidic chip, enabling a new type of post-stress measurements. Using this setup, we measured the H_2O_2 response of the green alga *C. reinhardtii* exposed to Cd^{2+} and CdSe/ZnS Qdots. In addition, intracellular ROS levels were measured and the dissolution of the Qdots was quantified by ICP-MS.

We found that algae can excrete overproduced ROS in the form of H_2O_2, sustaining constant intracellular ROS levels. Also, algae are able to reestablish their ROS/AOX balance after 60 min oxidative stress induced by Cd^{2+}. Furthermore, consecutive exposures induce enhanced H_2O_2 generation. CdSe/ZnS Qdots induce ROS generation in algae mainly due to the cell-associated Cd, whereas the effect of Zn is negligible. It is not entirely clear in which state (ionic or particulate) the Cd reacts with algae, but we confirmed an enhanced dissolution of Zn from Qdots in the presence of algae. Furthermore, we observed an induction time for the H_2O_2 release as compared to the Cd^{2+} experiments, suggesting Qdot dissolution prior to H_2O_2 generation. Finally, a decrease in extracellular H_2O_2 concentration was observed after 90 min exposure to 5 nM of Qdots, which we explained as H_2O_2 depletion through electron traps available on the surface of the Qdots with deteriorated shells. Overall, to the best of our knowledge, experiments with such complex exposure patterns are presented for the first time here. Of course, further investigations are necessary to elucidate the impact of Cd^{2+} and core/shell Qdots on living organisms. However, we demonstrated that our microfluidic platform opens the door for a completely new type of experiments, leading to a better understanding of ROS biology as well as to numerous opportunities for ecotoxicological studies.

Acknowledgements

The authors are very grateful to Prof. Sebastian Maerkl for the utilization of the microarray robot, to Prof. Christof Holliger for the access to the algae incubator and to Mr. Sylvain Coudret for assistance with ICP-MS.

Declaration of interest

The authors are responsible for writing of the article and report no conflicts of financial, consulting, and personal interests.

This work was supported by the Swiss National Research Program NRP 64 project no. 406440-131280/1 of the Swiss National Science Foundation.

References

Apel K, Hirt H. 2004. Reactive oxygen species: metabolism, oxidative stress, and signal transduction. Annu Rev Plant Biol 55:373–99.

Aravind P, Prasad MNV. 2005. Modulation of cadmium-induced oxidative stress in *Ceratophyllum demersum* by zinc involves ascorbate–glutathione cycle and glutathione metabolism. Plant Phys Biochem 43:107–16.

Bae Y, Myung N, Bard AJ. 2004. Electrochemistry and electrogenerated chemiluminescence of CdTe nanoparticles. Nano Lett 4:1153–61.

Balog S, Rodriguez-Lorenzo L, Monnier CA, Obiols-Rabasa M, Rothen-Rutishauser B, Schurtenberger P, Petri-Fink A. 2015. Characterizing nanoparticles in complex biological media and physiological fluids with depolarized dynamic light scattering. Nanoscale 7:5991–7.

Behra R. 1993. In vitro effects of cadmium, zinc and lead on calmodulin-dependent actions in Oncorhynchus mykiss, Mytilus sp., and *Chlamydomonas reinhardtii*. Arch Environ Contam Toxicol 24:21–7.

Bhatia SN, Ingber DE. 2014. Microfluidic organs-on-chips. Nat Biotechnol 32:760–72.

Bradac P, Navarro E, Odzak N, Behra R, Sigg L. 2009. Kinetics of cadmium accumulation in periphyton under freshwater conditions. Environ Toxicol Chem 28:2108–16.

Butt WD, Keilin D. 1962. Absorption spectra and some other properties of cytochrome c and of its compounds with ligands. Proc Royal Soc Lond B 156:429–58.

Clichici S, Filip A. 2015. In vivo Assessment of Nanomaterials Toxicity, Nanomaterials – Toxicity and Risk Assessment. Vienna: InTech, 92–120. .

Cooke MS, Evans MD, Dizdaroglu M, Lunec J. 2003. Oxidative DNA damage: mechanisms, mutation, and disease. FASEB J 17:1195–214.

Dabbousi BO, Rodriguez-Viejo J, Mikulec FV, Heine JR, Mattoussi H, Ober R, et al. 1997. (CdSe)ZnS core – shell quantum dots: synthesis and characterization of a size series of highly luminescent nanocrystallites. J Phys Chem B 101:9463–75.

Dar-Bin S, Chia-Chun H, Song-Bin H, Gwo-Bin L. 2009. A microfluidic-based cell culture platform for cellular and subcellular imaging. NEMS IEEE 4:223–6.

Dennany L, Gerlach M, O'Carroll S, Keyes TE, Forster RJ, Bertoncello P. 2011. Electrochemiluminescence (ECL) sensing properties of water soluble core-shell CdSe/ZnS quantum dots/Nafion composite films. J Mater Chem 21:13984–90.

Domingos RF, Simon DF, Hauser C, Wilkinson KJ. 2011. Bioaccumulation and effects of CdTe/CdS quantum dots on *Chlamydomonas reinhardtii* – nanoparticles or the free ions? Environ Sci Technol 45:7664–9.

Donaldson K, Stone V, Borm PJA, Jimenez LA, Gilmour PS, Schins RPF, et al. 2003. Oxidative stress and calcium signaling in the adverse effects of environmental particles (PM10). Free Radic Biol Med 34:1369–82.

Eggen RIL, Behra R, Burkhardt-Holm P, Escher BI, Schweigert N. 2004. Challenges in ecotoxicology. Environ Sci Technol 38:58A–64A.

El-Ali J, Sorger PK, Jensen KF. 2006. Cells on chips. Nature 442:403–11.

Finkel T, Holbrook NJ. 2000. Oxidants, oxidative stress and the biology of ageing. Nature 408:239–47.

Foyer CH, Noctor G. 2005. Redox homeostasis and antioxidant signaling: a metabolic interface between stress perception and physiological responses. Plant Cell Online 17:1866–75.

Garcia-Cordero JL, Maerkl SJ. 2014. A 1024-sample serum analyzer chip for cancer diagnostics. Lab Chip 14:2642–50.

Gill SS, Tuteja N. 2010. Reactive oxygen species and antioxidant machinery in abiotic stress tolerance in crop plants. Plant Physiol Biochem 48:909–30.

Gogos A, Knauer K, Bucheli TD. 2012. Nanomaterials in plant protection and fertilization: current state, foreseen applications, and research priorities. J Agric Food Chem 60:9781–92.

Gorrini C, Harris IS, Mak TW. 2013. Modulation of oxidative stress as an anticancer strategy. Nat Rev Drug Discov 12:931–47.

Govindarajan S, McNeil CJ, Lowry JP, McMahon CP, O'Neill RD. 2013. Highly selective and stable microdisc biosensors for l-glutamate monitoring. Sens Actuat B 178:606–14.

Grossman A. 2007. In the grip of algal genomics. In: León R, Galván A, Fernández E, eds. Transgenic Microalgae as Green Cell Factories. New York: Springer, 54–76.

Handy RD, Owen R, Valsami-Jones E. 2008. The ecotoxicology of nanoparticles and nanomaterials: current status, knowledge gaps, challenges, and future needs. Ecotoxicol 17:315–25.

Hanikenne M, Merchant SS, Hamel P. 2009. Chapter 10 – transition metal nutrition: a balance between deficiency and toxicity. In: Witman EH, ed. The Chlamydomonas Sourcebook. 2nd ed. London: Academic Press, 333–99.

He X, Pan Y, Zhang J, Li Y, Ma Y, Zhang P, et al. 2015. Quantifying the total ionic release from nanoparticles after particle-cell contact. Environ Pollut 196:194–200.

Henderson JR, Fulton DA, McNeil CJ, Manning P. 2009a. The development and in vitro characterisation of an intracellular nanosensor responsive to reactive oxygen species. Biosens Bioelectron 24:3608–14.

Henderson JR, Swalwell H, Boulton S, Manning P, McNeil CJ, Birch-Machin MA. 2009b. Direct, real-time monitoring of superoxide generation in isolated mitochondria. Free Radic Res 43:796–802.

Hu X, Han H, Hua L, Sheng Z. 2010. Electrogenerated chemiluminescence of blue emitting ZnSe quantum dots and its biosensing for hydrogen peroxide. Biosens Bioelectron 25:1843–6.

Huang L, Maerkl SJ, Martin OJF. 2009. Integration of plasmonic trapping in a microfluidic environment. Opt Express 17:6018–24.

Jiang H, Ju H. 2007. Enzyme-quantum dots architecture for highly sensitive electrochemiluminescence biosensing of oxidase substrates. Chem Comm 4:404–6.

Jin H, Heller DA, Kalbacova M, Kim JH, Zhang J, Boghossian AA, et al. 2010. Detection of single-molecule H2O2 signalling from epidermal growth factor receptor using fluorescent single-walled carbon nanotubes. Nat Nano 5:302–9.

Kalyanaraman B, Darley-Usmar V, Davies KJA, Dennery PA, Forman HJ, Grisham MB, et al. 2012. Measuring reactive oxygen and nitrogen species with fluorescent probes: challenges and limitations. Free Radic Biol Med 52:1–6.

Keeling PJ. 2004. Diversity and evolutionary history of plastids and their hosts. Am J Botany 91:1481–93.

Kim G, Lee YE, Kopelman R. 2013. Hydrogen peroxide (H_2O_2) detection with nanoprobes for biological applications: a mini-review. In: Armstrong D, Bharali DJ, eds. Oxidative Stress and Nanotechnology. New York: Humana Press, 101–14. .

Koman V, Suárez G, Santschi C, Cadarso VJ, Brugger J, von Moos N, et al. 2013. A portable microfluidic-based biophotonic sensor for extracellular H_2O_2 measurements. Proc SPIE 8572:857281–8.

Koman VB, Santschi C, Martin OJF. 2015a. Multiscattering-enhanced absorption spectroscopy. Anal Chem 87:1536–43.

Koman VB, Santschi C, von Moos NR, Slaveykova VI, Martin OJF. 2015b. Portable oxidative stress sensor: dynamic and non-invasive measurements of extracellular H_2O_2 released by algae. Biosens Bioelectron 68:245–52.

Lamelas C, Pinheiro JP, Slaveykova VI. 2009. Effect of humic acid on Cd(II), Cu(II), and Pb(II) uptake by freshwater algae: kinetic and cell wall speciation considerations. Environ Sci Technol 43:730–5.

Leptos KC, Guasto JS, Gollub JP, Pesci AI, Goldstein RE. 2009. Dynamics of enhanced tracer diffusion in suspensions of swimming eukaryotic microorganisms. Phys Rev Lett 103:198103–5.

Liu Y, Butler WB, Pappas D. 2012. Spatially selective reagent delivery into cancer cells using a two-layer microfluidic culture system. Anal Chim Acta 743:125–30.

Mahto SK, Charwat V, Ertl P, Rothen-Rutishauser B, Rhee SW, Sznitman J. 2014. Microfluidic platforms for advanced risk assessments of nanomaterials. Nanotoxicology 1:1–15.

Messner B, Ploner C, Laufer G, Bernhard D. 2012. Cadmium activates a programmed, lysosomal membrane permeabilization-dependent necrosis pathway. Toxicol Lett 212:268–75.

Misra SK, Dybowska A, Berhanu D, Luoma SN, Valsami-Jones E. 2012. The complexity of nanoparticle dissolution and its importance in nanotoxicological studies. Sci Total Environ 438:225–32.

Nathan C, Cunningham-Bussel A. 2013. Beyond oxidative stress: an immunologist's guide to reactive oxygen species. Nat Rev Immunol 13:349–61.

Navarro E, Baun A, Behra R, Hartmann N, Filser J, Miao AJ, et al. 2008. Environmental behavior and ecotoxicity of engineered nanoparticles to algae, plants, and fungi. Ecotoxicology 17:372–86.

Nel A, Xia T, Mädler L, Li N. 2006. Toxic potential of materials at the nanolevel. Science 311:622–7.

Nel A, Xia T, Meng H, Wang X, Lin S, Ji Z, Zhang H. 2013. Nanomaterial toxicity testing in the 21st century: use of a predictive toxicological approach and high-throughput screening. Acc Chem Res 46:607–21.

Nordberg GF, Fowler BA, Nordberg M. 2014. Handbook on the Toxicology of Metals. San Diego: Academic Press.

Nowack B, Bucheli TD. 2007. Occurrence, behavior and effects of nanoparticles in the environment. Environ Pollut 150:5–22.

Priester JH, Stoimenov PK, Mielke RE, Webb SM, Ehrhardt C, Zhang JP, et al. 2009. Effects of soluble cadmium salts versus CdSe quantum dots on the growth of planktonic *Pseudomonas aeruginosa*. Environ Sci Technol 43:2589–94.

Reiss P, Protière M, Li L. 2009. Core/shell semiconductor nanocrystals. Small 5:154–68.

Rodriguez-Lorenzo L, Rothen-Rutishauser B, Petri-Fink A, Balog S. 2015. Nanoparticle polydispersity can strongly affect in vitro dose. Particle Syst Character 32:321–33.

Sabella S, Carney RP, Brunetti V, Malvindi MA, Al-Juffali N, Vecchio G, et al. 2014. A general mechanism for intracellular toxicity of metal-containing nanoparticles. Nanoscale 6:7052–61.

Sharifi S, Behzadi S, Laurent S, Laird FM, Stroeve P, Mahmoudi M. 2012. Toxicity of nanomaterials. Chem Soc Rev 41:2323–43.

Slaveykova VI, Startchev K. 2009. Effect of natural organic matter and green microalga on carboxyl-polyethylene glycol coated CdSe/ZnS quantum dots stability and transformations under freshwater conditions. Environ Pollut 157:3445–50.

Slaveykova VI, Startchev K, Roberts J. 2009. Amine- and carboxyl-quantum dots affect membrane integrity of bacterium *Cupriavidus metallidurans* CH34. Environ Sci Technol 43:5117–22.

Suarez G, Santschi C, Slaveykova VI, Martin OJF. 2013. Sensing the dynamics of oxidative stress using enhanced absorption in protein-loaded random media. Sci Rep 3:52–7.

Sun Q, Wang XR, Ding SM, Yuan XF. 2005. Effects of interactions between cadmium and zinc on phytochelatin and glutathione production in wheat (*Triticum aestivum* L.). Environ Toxicol 20:195–201.

Tehranirokh M, Kouzani AZ, Francis PS, Kanwar JR. 2013. Microfluidic devices for cell cultivation and proliferation. Biomicrofluidics 7:5–9.

Thorsen T, Maerkl SJ, Quake SR. 2002. Microfluidic large-scale integration. Science 298:580–4.

von Moos N, Bowen P, Slaveykova VI. 2014. Bioavailability of inorganic nanoparticles to planktonic bacteria and aquatic microalgae in freshwater. Environ Sci Nano 1:214–32.

von Moos N, Slaveykova VI. 2014. Oxidative stress induced by inorganic nanoparticles in bacteria and aquatic microalgae-state of the art and knowledge gaps. Nanotoxicology 8:605–30.

Wang Y, Fang J, Leonard SS, Krishna RKM. 2004. Cadmium inhibits the electron transfer chain and induces reactive oxygen species. Free Radic Biol Med 36:1434–43.

Weinberg H, Galyean A, Leopold M. 2011. Evaluating engineered nanoparticles in natural waters. TrAC Trends Anal Chem 30:72–83.

Werlin R, Priester JH, Mielke RE, Kramer S, Jackson S, Stoimenov PK, et al. 2011. Biomagnification of cadmium selenide quantum dots in a simple experimental microbial food chain. Nat Nanotechnol 6:65–71.

Wu J, Chen Q, Liu W, Zhang Y, Lin JM. 2012. Cytotoxicity of quantum dots assay on a microfluidic 3D-culture device based on modeling diffusion process between blood vessels and tissues. Lab Chip 12:3474–80.

Yu BP. 1994. Cellular defenses against damage from reactive oxygen species. Phys Rev 74:136–92.

Zhang K, Chou CK, Xia X, Hung MC, Qin L. 2014. Block-cell-printing for live single-cell printing. Proc Natl Acad Sci USA 111:2948–53.

Zhang LW, Monteiro-Riviere NA. 2009. Mechanisms of quantum dot nanoparticle cellular uptake. Toxicol Sci 110:138–55.

Supplementary material available online

Supplementary Tables S1–S6 and Figures S1–S7